Applied Surface Science Advances 6 (2021) 100157

Contents lists available at ScienceDirect

Applied Surface Science Advances

journal homepage: www.sciencedirect.com/journal/applied-surface-science-advances

Adsorption of antiretroviral drugs, efavirenz and nevirapine from aqueous solution by graphene wool: Kinetic, equilibrium, thermodynamic and computational studies

Adedapo O. Adeola, Jurgens de Lange, Patricia B.C. Forbes *

Department of Chemistry, Faculty of Natural and Agricultural Sciences, University of Pretoria, Lynnwood Road, Hatfield, Pretoria 0002, South Africa

ARTICLE INFO

Keywords:
Antiretroviral drug
Efavirenz
Nevirapine
Emerging contaminant
Graphene wool

ABSTRACT

The increasing concentrations of pharmaceutical and personal care products in water bodies have attracted attention due to the risk of non-target exposures. The application of any graphene-based material for the remediation of antiretroviral drug contamination has not been reported, therefore graphene wool was synthesized by chemical vapour deposition as adsorbent for the removal of efavirenz (EFV) and nevirapine (NVP) from water. Results revealed that adsorption of EFV was best fitted to the intraparticle diffusion model, with multilinearity (multiple adsorption steps). The pseudo-second-order model best describes GW-NVP interaction. Isotherm parameters revealed that Sips and Freundlich model best fit GW-EFV and GW-NVP interactions, with the least value of SSE < 0.04 and 1.27, respectively. GW demonstrated higher adsorption capacity and adsorption maxima for NVP with K_d and q_m values of $\sim$ 2.54 L/g and $\sim$ 48.31 mg/g, compared to $\sim$ 1.48 L/g and $\sim$ 4.41 mg/g obtained for EFV adsorption. Isotherm parameters suggest that GW adsorbed NVP slightly better with stronger binding strength than EFV, with removal efficiencies of 84% (NVP) and 80% (EFV) under optimum conditions. A heterogeneous adsorption mechanism was suggested for GW-EFV sorption, in contrast to a less heterogeneous and multilayer adsorption mechanism for GW-NVP adsorption. NVP adsorption is a spontaneous exothermic process, while GW-EFV interaction is a spontaneous endothermic process. Experimental results were supported by computational studies, which revealed the influence of strong dispersion interactions and H-bonding at specific pH ranges.

1. Introduction

Pharmaceuticals and personal care products (PPCP) are a vast and unique class of emerging chemical pollutants (ECP). They may cause physiological effects and alter systemic processes in humans upon exposure to low concentrations, which makes non-target exposures worrisome [1, 2]. In the last decade, the occurrence of antiviral and antiretroviral drugs as microcontaminants in drinking and surface water has received significant attention in both developing and developed parts of the world [3-6]. The risk assessment and adverse effects of exposure to these chemicals are not fully understood, but there is growing scientific, public, and regulatory concern as these drug compounds have been detected in surface waters [7-9]. The toxicological profile of selected antiviral drugs suggests that they are hazardous to aquatic fauna, with a low maximal effective concentration (EC_{50}) value of 57 mg/L [4]. Several antiviral drugs and their metabolites are nonbiodegradable, hence they persist in the environment [6, 10].

Antiretroviral drugs (ARVDs) are therapeutic agents for the treatment of retroviral infections, primarily the human immunodeficiency virus type 1 (HIV-1). The virus that causes HIV disease attacks the CD4-T cells responsible for body immunity, thus making humans vulnerable or susceptible to infections and diseases [11-12]. Antiretroviral treatment therapy against HIV-1 does not eliminate the virus but inhibits its rapid replication and increases the life expectancy of infected people [13].

This page is inserted as it is not possible to submit just a revised version of the manuscript with changes shown in red. It is mandatory on your system to submit a "Revised manuscript (clean version)", which was done. However we received a request twice thereafter for the same revision to "Please remove the former manuscripts. Please keep only one manuscript, the one that contains the corrections marked in red colour." The former manuscript was removed during the first revision already.

* Corresponding author.
E-mail address: patricia.forbes@up.ac.za (P.B.C. Forbes).

https://doi.org/10.1016/j.apsadv.2021.100157
Received 24 May 2021; Received in revised form 13 August 2021; Accepted 30 August 2021
Available online 8 September 2021

Table 1
Physicochemical properties of target antiretroviral drugs (ARVD).

ARVD (and abbreviation)	Molecular formula	LogK_{ow}	S_w	MM	pKa
Efavirenz (EFV)	$C_{14}H_9ClF_3NO_2$	4.70	0.093	315.68	10.20/ 12.52
Nevirapine (NVP)	$C_{15}H_{14}N_4O$	3.89	0.705	266.30	2.80

Log K_{ow}: octanol–water partition coefficient, S_w: water solubility (mg/L), MM: molar mass (g/mol), pKa:-log of acid-dissociation constant. Cited from pubchem [25, 26].

About 90% of orally administered drugs are removed unaltered or partially metabolized from the body as faecal waste, and they are thus found in sewage waste [14]. Similarly, unused and expired drugs may be disposed indiscriminately resulting in contamination of drainage systems and other water bodies [15].

Efavirenz and nevirapine exert distinct pathways for the inhibition of the proliferation of HIV, and they are classified amongst the most common ARVDs [16]. Adsorption of efavirenz onto biosolids has reportedly enhanced the removal efficiency of ARVDs in conventional wastewater treatment plants (WWTPs) in South Africa, with an efavirenz sludge concentration as high as 43 mg/kg, while 22.5% removal efficiency of nevirapine was also reported [17]. A Kenyan study reported decontamination efficiencies of 11 – 49% (nevirapine) and 83 – 92% (efavirenz) in three WWTPs [18]. Premised on the bioactivities of PCPPs at very low concentrations, non-target exposures via drinking water supplies and improper waste disposal, the inefficient performance of many existing wastewater and sewage treatment plants (WWTPs & STPs), and toxicities of pharmaceutical products; there is a need for more research on sustainable, efficient and ecofriendly remediation approaches (such as adsorption processes, green bioremediation, etc.) for removal of ARVDs from aqueous systems.

Adsorption techniques arising from material science advances have proven useful in mitigating the challenge of emerging chemical pollutants (such as pharmaceuticals) in water [19-21]. The adsorption method for the decontamination of water polluted with organic chemical pollutants has benefits such as simplicity in design and operation, low operational cost, easy adaptability, and minimal tendency of generating secondary pollutants or undesirable by-products [22-24]. Graphene-based materials (GBMs) have been harnessed as efficient next-generation sorbents for water purification applications, because their surface is largely hydrophobic, porous, and possesses high adsorption affinities for a vast number of organic contaminants (OCs) [19, 21, 22]. However, the application of graphene-based materials for the remediation of any antiretroviral drug contamination in water has not been reported previously.

Therefore, the overall aim of this study was to synthesize graphene wool (GW) for the removal of selected ARVDs from an aqueous solution. Sorption isotherm, kinetics, thermodynamic and computational studies were carried out to elucidate and evaluate the sorption mechanism(s) of GW-ARVD interactions, as well as the adsorption capacities and removal efficiency of graphene wool for potential use in the purification of ARVD-contaminated water. **Table 1** provides a summary of the basic physicochemical properties of the target ARVDs chosen for this study. Efavirenz and nevirapine were chosen as target antiretroviral drugs based on their toxicity, prevalence and persistence in surface waters [4].

2. Experimental methods

2.1. Synthesis of graphene wool (GW)

Graphene wool was synthesized using an established bottom-up approach as reported in [27]. Briefly, quartz wool (Arcos Organics, New Jersey, USA) was carefully arranged at the centre of a horizontal quartz tube (50 mm o.d., 44 mm i.d., x 1 m length) in a high-temperature furnace (OTF-1200X-50–5 L, MTI Corporation, California, USA). 500 sccm argon and hydrogen (analytical grade, 99.999%, Afrox, South Africa) were pre-mixed and released into the thermal reactor at 1200 °C. The quartz wool was annealed under this temperature and gas flow for 10 min, thereafter methane gas (analytical grade, 99.95%, Afrox, South Africa) was added for graphene growth. The system was cooled under Ar and H_2 gas after the optimized growth time had elapsed. Thus, the graphene wool (GW) synthesized is a composite of quartz wool coated with graphene.

2.2. Characterisation of graphene wool (GW) adsorbent

Surface morphology was examined using scanning electron microscopy (SEM) with aid of a Zeiss Ultra-Plus 55 field emission scanning electron microscope (FE-SEM), operated at 2.0 kV (OXFORD Link-ISIS-300 Zeiss, Germany); High-resolution transmission electron microscopy (TEM) images were taken using a JEOL JEM 2100F (JOEL Ltd, Tokyo, Japan) operated at 200 kV. The crystal structure of GW was also examined using a Bruker BV 2D Phaser X-ray diffraction (XRD) instrument with reflection geometry at 2θ values (10 – 60°) with a 5.24 s requisition time per step, operated with a Cu $K\alpha_1$ radiation source (λ = 0.15406 nm) at 50 kV and 30 mA. The surface area and porosity of GW were determined by N_2 adsorption-desorption isotherms at 77 K, using a NOVA Touch Surface analyzer system (Anton Paar, South Africa) in a relative pressure (P/P_0) range of 0.01−1.0, following a model of Brunauer−Emmett−Teller (BET) and Barrett−Joyner−Halenda (BJH) techniques

2.3. Adsorption kinetics and isotherm experiments

Batch adsorption experiments of efavirenz (EFV) and nevirapine (EFV) onto GW adsorbent were carried out in 40 mL PTFE screw-capped vials (Stargate Scientific, South Africa) at 25 ± 1 °C. Background electrolyte contained 0.01 mol/L $CaCl_2$ (analytical grade, ACE, South Africa) in deionized water (9.2 μS/cm^3, Millipore, Bedford, MA, USA), and 200 mg/L NaN_3 (analytical grade, Sigma-Aldrich, Germany) to inhibit microbial activity. Kinetic experiments were conducted for 72 h with initial EFV and NVP concentrations of 5 mg/L (99% pure standards, analytical grade were purchased from Sigma-Aldrich, Germany), and the mass per volume ratio was 10 mg of graphene wool per 5 mL solution.

Afterwards, the isotherm experiments were carried out with initial concentrations of ARVD solutions ranging between 1 - 20 mg/L, respectively. Desorption experiments were carried out by adding fresh 5 mL of background electrolyte after the supernatant from the adsorption studies had been decanted. Sorption thermodynamic evaluations were carried out at varying temperatures of 298, 308, and 318 K using a thermostated shaking water bath (Wisebath, Celsius Scientific, South Africa). The role of solution pH was studied over the pH range of 2 - 13, and the pH of the solutions was adjusted using 0.1 M HCl (analytical grade, Merck, South Africa) and/or 0.01 M NaOH (analytical grade, ACE, South Africa). Adsorption performance of GW for the removal of EFV and NVP was also studied at varying contact times (0, 15, 30, 60, 120, 240, 360, 600, 840, 1440, 2160, 2880, 3600, and 4320 mins, respectively). All experiments were carried out in duplicate.

2.4. Quantification

After equilibration for 24 h, the vials were centrifuged at 3000 rpm for 5 min to obtain a clear supernatant, which was then filtered using a 0.22 μm syringe filter (Stargate scientific, South Africa) and collected in 2 mL LC vials for analysis by ultra-performance liquid chromatography coupled with tandem mass spectrometry (UPLC-MS/MS).

2.4.1. UPLC-MS/MS analysis

Analysis of the supernatant was carried out using sensitive and rapid ultra-performance liquid chromatography (UPLC); accompanied by

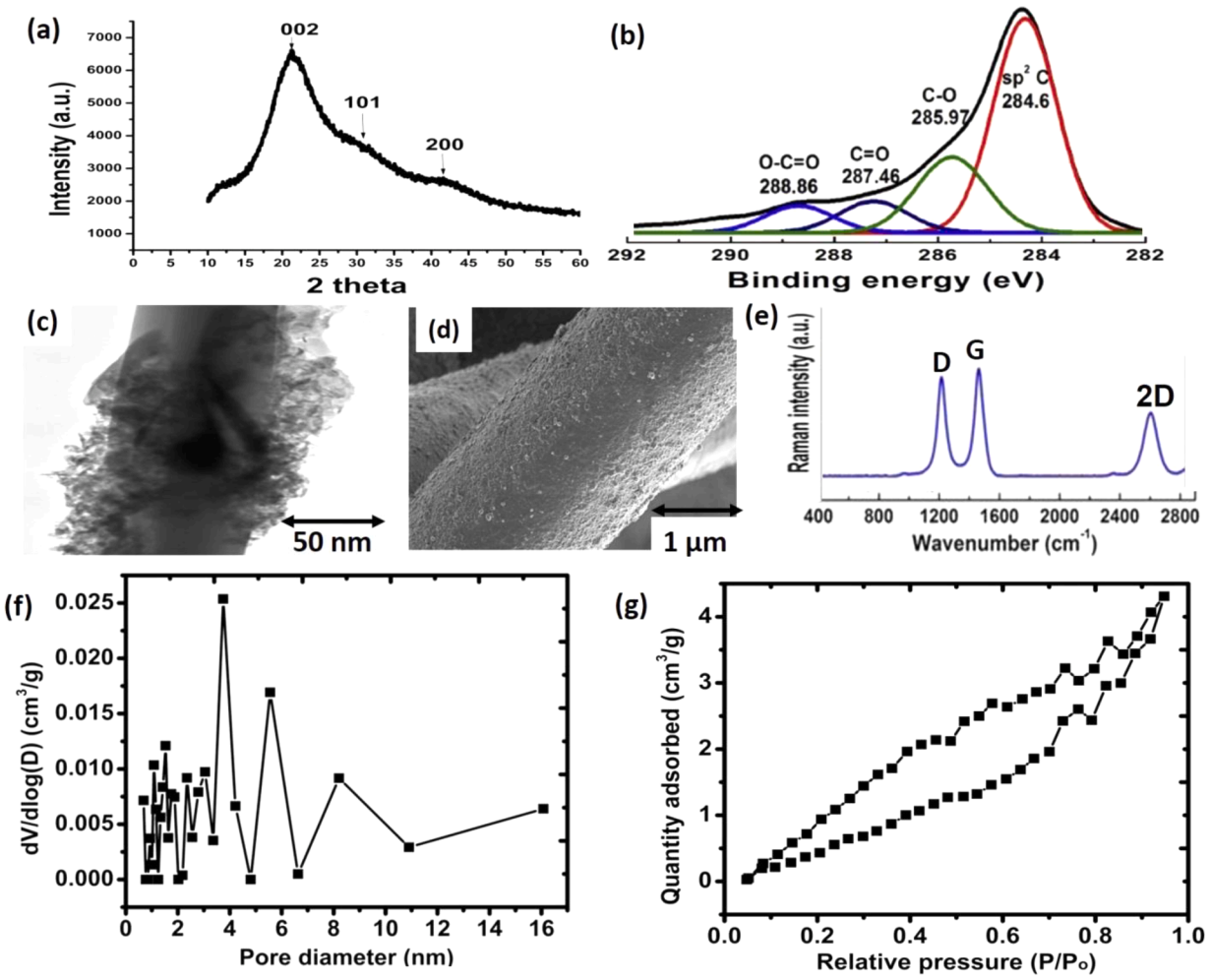

Fig. 1. Characterisation of graphene wool adsorbent, (a) XRD pattern (b) XPS spectrum (c) TEM image (d) SEM image (e) Raman spectrum showing the D, G and 2D peaks unique to multilayer graphene (f) Pore size distribution of GW and (g) N_2-sorption isotherm obtained from BET analysis.

electrospray ionization (ESI) in positive and negative mode (NVP and EFV, respectively) and mass spectrometric (MS) detection with a triple-quadrupole MS/MS system (Waters Inc., Milford, Massachusetts, USA). Chromatographic separation was achieved using an Acquity UPLC® ethylene bridged hybrid (BEH) shield reversed-phase C18 column (1.7 µm particle size, 100 mm length × 2.1 mm internal diameter) equipped with an Acquity UPLC C18 guard column (Waters, Milford, MA). EFV and NVP separation was carried out with 0.1% formic acid (HPLC grade) in water (solvent A) and 0.1% formic acid in acetonitrile (solvent B, HPLC grade), while the temperature of the column was maintained at 40 °C, the flow rate was set at 0.3 mL/min and a gradient run time of 5 min. The LC system was equipped with an autosampler with 5 µL injection volume per analysis, and samples were analysed in duplicate ($n = 2$) and standards in triplicates ($n = 3$). The MS discharge electrode was set at 5 µA for electrospray negative and positive ionization for EFV and NVP, respectively; the gas temperature was set at 250 °C, sheath gas temperature at 300 °C, the gas flow rate was set at 10 L/min, Delta EMV set at 400 V, nebuliser pressure of 35 psi, and capillary voltage was set at 3000 V.

Data acquisition and analysis was carried out using MassLynx™ (version 4.2) software (Waters, Milford, MA) and QuanLynx Method Editor V4.2 was used to prepare the calibration curve and quantification of EFV and NVP. The calibration curves were obtained from stock solutions of each ARVD with regression coefficient (R^2) > 0.98. The working standards were in the range of 0.01 – 5 mg/L for EFV and NVP, respectively. Equilibrium concentrations (C_e) were deduced from the equation of the curve and the amount adsorbed was calculated using the mass-balance equation presented below:

$$q_e = \frac{(C_0 - C_e)V_0}{S_m} \quad (1)$$

Where C_o (mg/L) is the initial concentration, C_e (mg/L) is the equilibrium solute concentration, V_o is the initial volume (L) and S_m is the mass (g) of the adsorbent.

$$\text{Removal efficiency } (\%) = \frac{(C_0 - C_e)}{C_0} \times 100 \quad (2)$$

2.5. Computational study of GW-ARVD interaction

EFV and NVP, in various conformers and tautomers, were optimized with Density Functional Theory (DFT), using B3LYP/6–31G(d) and the conductor-like polarizable continuum solvation model (CPCM) with water. Interactions between EFV, NVP, and various forms of a 5 × 5 graphene sheet (including functionalization with –O and –OH groups) were optimized. All structures are true local energy minima unless otherwise noted. All electronic structure calculations were performed with Gaussian 16, rev. C [28]. Selected wavefunctions were further investigated with the Fragment, Atomic, Localized, Delocalized and Interatomic (FALDI) density decomposition scheme [29, 30] using in-house codes and in conjunction with atomic basins defined by the Quantum Theory of Atoms in Molecules (QTAIM) [31], as implemented

Table 2
Kinetic parameters for efavirenz and nevirapine adsorption by graphene wool (GW) adsorbent and sum of square of errors (SSE) from nonlinear regression analysis.

Adsorption kinetics	Parameter	ARVD Efavirenz (EFV)	Nevirapine (NVP)
First order	*Predicted q_e (mg/g)*	1.193	3.269
	Experimental q_e (mg/g)	1.956	4.717
	K_1 (1/min)	1.017	1.000
	SSE	**1.180**	**1.237**
Second order	*Predicted q_e (mg/g)*	1.494	4.730
	Experimental q_e (mg/g)	1.956	4.717
	K_2 (mg/g.min)	0.040	0.007
	h (mg/g.min)	0.090	0.220
	Half-life ($t_{0.5}$)	16.670	21.140
	SSE	**0.830**	**0.288**
Weber-Morris intraparticle diffusion	*K_{id} (mg/g.min$^{1/2}$)*	0.022	0.051
	C	0.821	2.375
	SSE	**0.306**	**0.441**

in AIMAll v. 19.10.12 [32]. FALDI was used to calculate and visualize inter-fragment delocalization indices (DIs), through the joint overlap of atomic overlap matrices. FALDI delocalization indices (DIs) were performed without the localized-delocalized overlap correction [30] and correspond to orthodox QTAIM-defined DIs. Visualizations of FALDI fields were performed with visual molecular dynamics (VMD) [33].

3. Results and discussion

3.1. Characterisation of graphene wool

Figure (1a) reveals that graphene wool (GW) has an amorphous structure with an intercellular spacing of d_{002} = 3.70 Å, confirmed by the broad diffraction plane C (002) appearing at 2θ = 22.5°. The shift of carbon plane (002) to lower Bragg angle (26.4° to 22.5°) and broad peak confirms the coverage of the wool substrate by several layers of graphene, thus creating an amorphous carbon phase [34]. The hump nature of the diffraction pattern is a result of the presence of amorphous silica substrate with weak peaks at 30° and 42° respectively [35, 36]. The XPS and Raman spectra (Fig. 1**b** & 1**e**) revealed sp^2 $C = C$ structure as the most intense peak at 284.6 eV, which reflects a partially disordered network of the graphene multilayer structure and accounts for the D peak in the Raman spectrum (Fig. 1**e**) [27, 37-39].

The SEM and TEM analysis provided high-resolution microscopic images of GW (Fig. 1**c** & 1**d**). The analysis revealed that the diameter of each strand of GW is between 6 - 8 μm and extensive coverage of the substrate by graphene, with a rough and heterogeneous surface morphology. The BET analysis revealed a H4-isotherm curve associated with complex materials/composites (Fig. 1**f**) and the pore size distribution plot (Fig. 1**g**) showed that GW adsorbent has both micropores (pore diameter > 2 nm) and mesopores (2 nm < pore diameter < 50 nm), but no macropores [39]. The specific surface area (SSA), pore volume, and pore diameter were 29.6 m^2/g, 0.039 cc/g, and 1.37 nm respectively.

3.2. Adsorption kinetics and effect of contact time

The pseudo-first-order (PFO) eq. (3)), pseudo-second-order (PSO) (eq. (4)), and Weber-Morris intraparticle diffusion (eq. (5)) models were used to fit the time-concentration profile of adsorption of efavirenz and nevirapine onto synthesized graphene wool adsorbent (Fig. 1). Reaction pathways in adsorption processes are influenced by contact time. The sorption rate and mechanisms of adsorption can be deduced from time-concentration data derived from sorbate-sorbent interaction prior to equilibrium [41, 42]. The initial adsorption rate and half-life were also calculated (eq. (6) and (7) and the models were validated using the sum of square of errors (SSE) (eq. (8)) [40–42]. The kinetic parameters obtained from the models are presented in **Table 2**.

$$q_t = q_e\left(1 - e^{-K_1 t}\right) \tag{3}$$

$$q_t = \frac{q_e^2 K_2 t}{q_e K_2 t + 1} \tag{4}$$

$$q_t = K_{id} t^{0.5} + C \tag{5}$$

$$h = K_2 q_e^2 \tag{6}$$

$$t_{0.5} = \frac{1}{K_2 q_e} \tag{7}$$

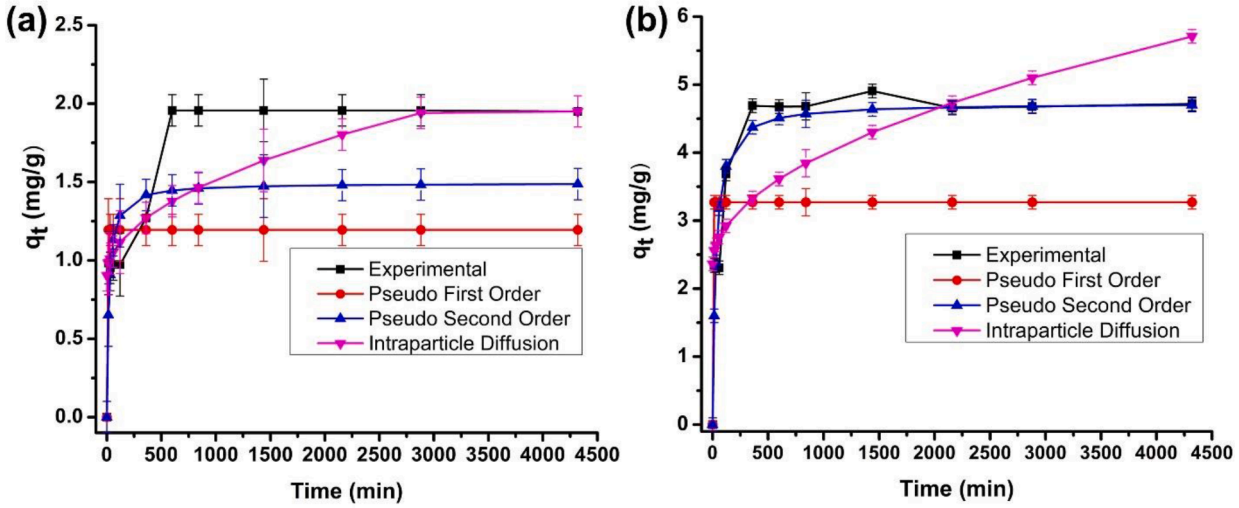

Fig. 2. Lagergren pseudo-first-order, pseudo-second-order and Weber-Morris intraparticle diffusion models of adsorption of (a) efavirenz and (b) nevirapine; onto graphene wool (Experimental conditions: Co = 5 mg/L; dosage = 10 mg per 5 mL, mixing rate = 200 rpm, T = 25 ± 1 °C). Error bars show ± relative standard deviation.

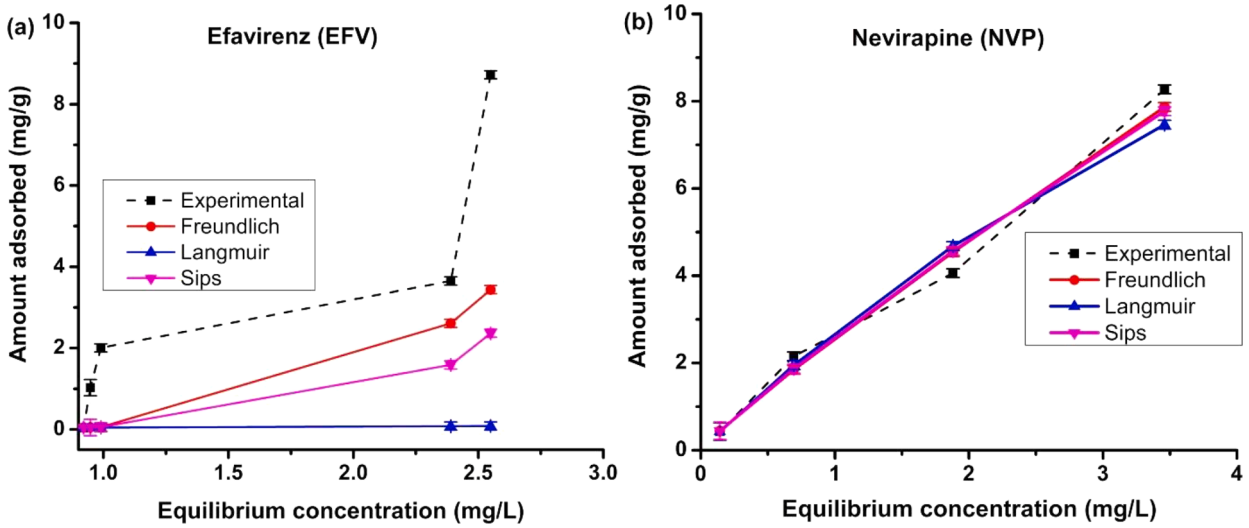

Fig. 3. Plots of sorption isotherm model for (a) efavirenz (EFV) adsorption and (b) nevirapine adsorption onto GW adsorbent (Experimental conditions: $C_o = 1 - 20$ mg/L; dosage = 10 mg per 5 mL, mixing rate = 200 rpm, $T = 25 \pm 1$ °C). Error bars show ± relative standard deviation.

Table 3
Coefficients obtained for sorption isotherm models for selected antiretroviral drugs adsorption by graphene wool (GW) and sum of square of errors (SSE) (Experimental conditions: dosage = 20 mg per 10 mL; mixing rate = 200 rpm; $T = 25 \pm 1$ °C; initial conc.: 1 - 20 mg/L; contact time = 24 h).

Isotherm model	Parameter	Efavirenz	Nevirapine
Linear	K_d *(L/g)*	1.482	2.544
	SSE	1.368	0.093
Freundlich	*N*	1.263	0.902
	K_F	1.269	2.569
	SSE	1.295	0.038
Langmuir	q_{max} *(mg/g)*	8.99e2	25.547
	K_L *(L/mg)*	0.002	0.119
	R_L	0.940	0.248
	SSE	1.370	0.042
Sips	*ms*	23.503	0.945
(Freundlich-Langmuir)	K_s *(L/mg)*	1.065	0.058
	q_m *(mg/g)*	4.408	48.313
	SSE	1.263	0.039

$$\sum_{i=1}^{n} \left(q_{e,cal} - q_{e,\ exp}\right)_i^2 \tag{8}$$

Where q_t and q_e are the amount of adsorbate sorbed per mass of adsorbent (mg/g) at a time (t) and equilibrium, respectively; K_1 (1/min) and K_2 (g/mg × min) are pseudo-first-order and pseudo-second-order rate constants, respectively; K_{id} (mg/g × $min^{1/2}$) and C (mg/g) are the intraparticle diffusion rate constant and constant associated with boundary layer thickness, respectively; and h (μg/g × min) and $t_{0.5}$ are the initial adsorption rate and half-life, respectively.

Table 2 revealed that the adsorption of efavirenz and nevirapine are best fitted to intraparticle diffusion and pseudo-second-order (PSO) kinetic models, given the lowest values of SSE. Fig. 2**(a)** revealed that EFV adsorption patterns exhibit multiple linearities, suggesting that several steps governed the GW-EFV interaction. The boundary layer constant (C) is both greater than zero for GW-EFV and GW-NVP which suggests that other mechanisms aside from film diffusion occurred during adsorption of both sorbates [41]. The initial steps include bulk transport and film diffusion between the sorbent-solution boundary layer, followed by adsorption of EFV onto pores of GW [41, 43]. The SSE suggests that even though the intraparticle diffusion model also fit GW-NVP interaction, the pseudo-second-order (PSO) model best describes the adsorption pathway for nevirapine (Fig. 2**b**). This suggests that some degree of chemical adsorption took place and contributed significantly to the adsorption rate and mechanism for NVP uptake. The predicted and experimental amount adsorbed (q_e) for nevirapine are of similar magnitude (47.3 and 47.2), which further confirms that PSO best fits GW-NVP interaction.

The initial steepness observed in Fig. 2 in the first 240 min of contact, reflects fast initial adsorption due to availability of GW sorption sites to the respective ARVDs, before a period of slow adsorption as available sites diminish, and equilibrium is reached after site saturation. The GW-EFV and GW-NVP reached equilibrium after 600 min and 360 min, respectively. The initial rate constant (h) reveals that the rate of adsorption of nevirapine is faster than efavirenz in the first 120 mins (Table 2), which could be attributed to lower molecular weight (size), availability of lone electron pairs, and π-electrons for binding interactions with GW. However, the PSO overall rate constant (K_2) suggests that EFV had a faster diffusion-controlled rate of adsorption, which was faster than the rate of chemisorption governing the adsorption of NVP [42, 44].

3.3. Adsorption isotherm

Adsorption isotherms provide vital information on the nature of the interaction between sorbates and sorbents, especially the amount of analyte adsorbed, and the amount unadsorbed after equilibrium is reached [40]. Linear regression and nonlinear isotherm models such as Linear (eq. (9)), Freundlich (eq. (10)), Langmuir (eq. (11)), and Sips model (eq. (13)) were used to fit adsorption experimental data. The sum of square of errors (SSE) (eq. (8)) was used to test all models used in this study [44, 45].

$$q_e = K_d C_e \tag{9}$$

$$q_e = K_F C_e^N \tag{10}$$

$$q_e = \frac{q_{max} K_L C_e}{1 + K_L C_e} \tag{11}$$

$$R_L = \frac{1}{1 + K_{Lq_{max}} C_0} \tag{12}$$

$$q_e = \frac{q_m K_s C_e^{ms}}{1 + K_s \cdot C_e^{ms}} \tag{13}$$

where K_F (mg/g) $(L/mg)^N$) and N (dimensionless) are the Freundlich constant and intensity parameter, an indicator of site energy

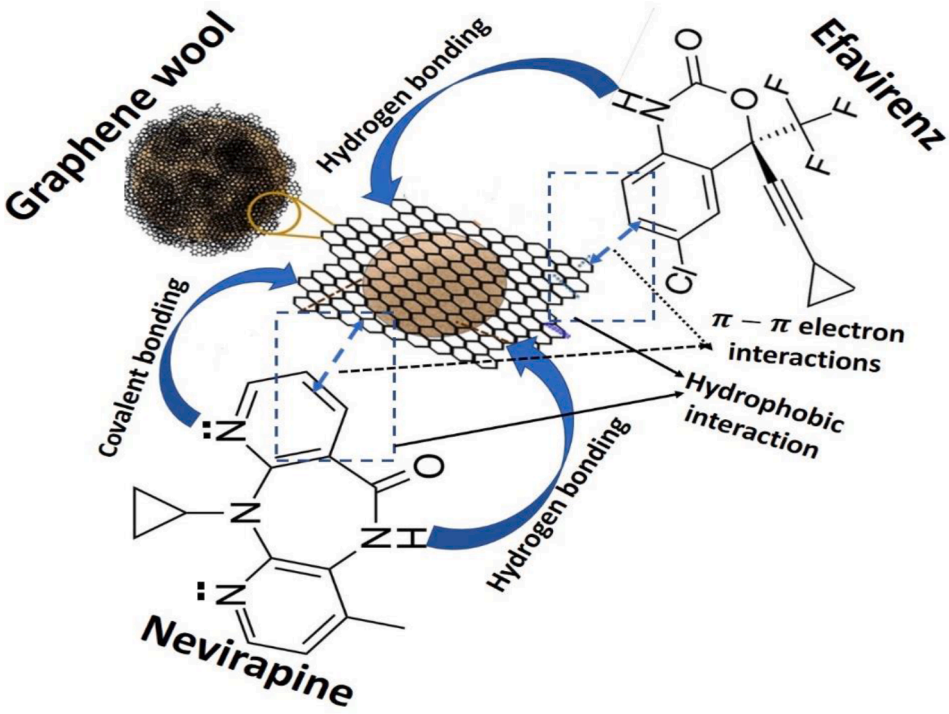

Fig. 4. Probable mechanisms of interaction between graphene wool and selected ARVDs.

Table 4
Sorption-desorption parameters and hysteresis index (*H*) derived from Freundlich isotherm model.

Sorbates	$K_{f.des}$	N_{ads}	N_{des}	SSE	R^2	*H
Efavirenz	0.70	1.26	4.39	1.50	0.992	0.29
Nevirapine	4.29	0.90	1.21	0.17	0.997	0.74

**H*: Sorption–desorption hysteresis index, $H = N_{ads}/N_{des}$; $\boldsymbol{N_{(ads)}}$: *Freundlich adsorption intensity,* $\boldsymbol{N_{(des)}}$: *Freundlich desorption intensity*.

heterogeneity; q_{max} (mg/g) and K_L (L/mg) are the Langmuir maximum adsorption capacity and Langmuir constant associated with solute–surface interaction energy, respectively; K_s (L/mg) *and* q_{max} (mg/g) are Sips isotherm model constants and maximum adsorption capacity and *ms* is Sips isotherm exponent; q_e is the solid-phase concentration (mg/g), C_e is the liquid phase equilibrium concentration (mg/L), and K_d (L/g) is the sorption distribution coefficient [22, 40]. The value of the separation factor R_L (eq. (12)) provides important information about the nature of adsorption; ($R_L < 1$ = favourable adsorption; $R_L > 1$ = unfavourable adsorption; $R_L = 1$ = linear adsorption; $R_L = 0$ = irreversible) [,][37,38].

The one, two, and three-parameter models used in this study provided useful insight into the nature and mechanism of adsorption of the selected ARVDs by graphene wool; and nonlinear regression analysis of experimental data using equations (9 - 13), have been reported to provide a more accurate fit than linear regression [44, 45]. Isotherm data for EFV was best fitted by Sips isotherm model with least SSE < 1.27, while NVP was best described by a multilayer adsorption mechanism depicted by Freundlich model with SSE < 0.039, respectively (Fig. 3, Table 3).

Sips is a hybrid of the Langmuir and Freundlich model and describes heterogeneous adsorption systems [45]. Thus, given that it best fit EFV adsorption, this implies that the interaction of EFV with GW is complex and highly heterogeneous, which accounts for the comparatively high heterogeneity (*N & ms*) index (Table 3). Basic models such as Freundlich and Langmuir would not completely describe the EFV sorption mechanism, due to limitations caused by increased adsorbate concentration and the nature of solute normally associated with the Freundlich model [45, 46]. Therefore, at low adsorbate concentration, the Sips model could reduce to Freundlich model (multilayer adsorption), and at high concentration of adsorbate, it predicts Langmuir model (monolayer adsorption).

The solute–surface interaction energy (K_L), Sips maximum adsorption capacity (q_m) and adsorption capacities (K_d & K_F) revealed that NVP has stronger binding strength and higher sorption capacity onto GW adsorbents, while GW-EFV interaction is mainly dominated by weak van der Waal's and hydrophobic bonding interactions considering its hydrophobicity (Log*Kow*) and structure (Table 1).

3.3.1. *Plausible sorbent-sorbate mechanism of interaction*

The mechanism of interaction between adsorbents and adsorbates is often influenced by the moieties/functional groups and molecular/electronic conformation of the adsorbents and adsorbates. The bulky molecular nature of organic compounds including pharmaceuticals often leads to several competing interactions. In this study, the Sips model described the adsorption of EFV and NVP onto GW well, which affirms the existence of complex interactions, which can be influenced by concentrations of target compounds, solution's pH, and temperature of the system. The electron pairs on the nitrogen atom in the pyridine aromatic structure present in nevirapine, suggest possible covalent bonding interactions between NVP and electrophiles without disruption of the aromatic ring of NVP. This provided a plausible explanation for the stronger interaction between GW-NVP than GW-EFV as presented by isotherm data (Table 3).

Other non-covalent bonding interactions are probable between GW-EFV and GW-NVP, and they include binding mechanisms such as π-π stacking, hydrogen bonding, van der Waals and hydrophobic bonding (Fig. 4), which have been reported to control the adsorption of several organic pollutants by graphene-based materials [47-49]. Furthermore, the presence of electronegative atoms such as fluorine, chlorine, and nitrogen in the target compounds, as well as the proton-rich structure of graphene; indicate that electrostatic attraction and repulsion in ionic aqueous medium cannot be ruled out, especially under varying pH [50].

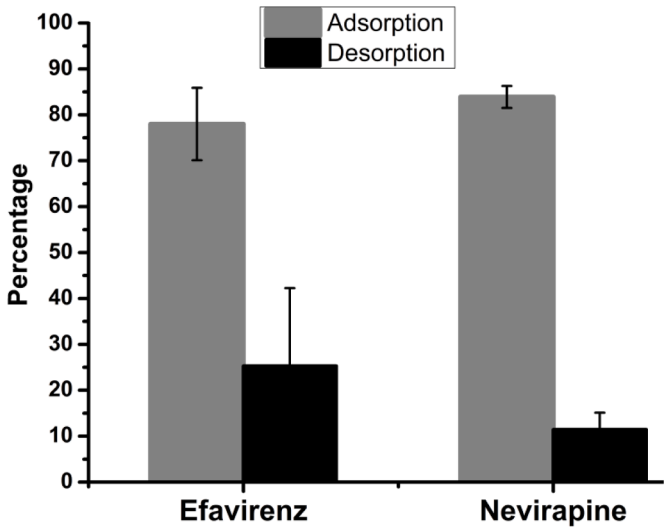

Fig. 5. Percentage adsorption and desorption of efavirenz (EFV) and nevirapine (NVP) by graphene wool (GW). Error bars show ± standard deviation, $n = 5$.

3.4. Desorption isotherm and hysteresis

The release and subsequent recontamination potential of adsorbed compounds are often evaluated by desorption studies. Thus, evaluating the fraction of adsorbed EFV and NVP, that can desorb into an aqueous solution by reaching a new equilibrium is vital for GW industrial application and decontamination processes [41]. Hysteresis index (H), which is a measure of the irreversibility of the sorption process, was calculated for GW-EFV and GW-NVP interactions. Table 4 revealed H-index values for both ARVDs were greater than zero ($1/N_{ads} > > > 1/N_{des}$), which implies that some degree of sorption–desorption hysteresis occurred [51].

The calculated hysteresis index was greater in GW-NVP, which suggests a higher tendency for irreversible sorption (hysteresis) in GW-NVP sorption-desorption interaction (Table 4). This can be attributed to stronger binding strength and possible sorption site defects and entrapment of adsorbed molecules [41, 52]. Experimental data revealed that more of NVP was adsorbed as clearly observed in the isotherm parameters, with significantly higher binding capacity (Table 2 and Fig. 5). On the contrary, GW-EFV displayed higher values of heterogeneity index (N_{ads} and N_{des}) suggesting a heterogeneous interaction, which potentially leads to sorption disequilibrium, weaker binding capacity, and faster rate of desorption of adsorbed molecules. Fig. 5 revealed that the % adsorption and desorption for efavirenz are 80 and 25.3%, and nevirapine are 84 and 11.5%, respectively. Nevirapine displayed weaker desorption potential which suggests stronger binding strength between nevirapine and GW (Fig. 5).

3.5. Effect of pH on adsorption of selected ARVDs

The need to study the influence of pH on the adsorption of organic pollutants including PPCPs, in contaminated aqueous solution is germane towards predicting optimum process conditions. The presence of specific moieties such as -OH, -COOH, -NH groups in many pharmaceutical products ensures protein-binding and transport in blood for pharmacological action and therapeutic effects [53], however, these functionalities make them susceptible to deprotonation under variable pH conditions. Furthermore, pKa values of efavirenz and nevirapine are presented in Table 1, and many notable reports have affirmed that the acid dissociation constant (pKa) largely influences the effect of pH on sorption processes of PCPPs, as pH range determines when the bulky compound is cationic or anionic in aqueous solution [54-56]. Generally, solution pH alters the surface properties of adsorbents and speciation of the compounds in the solution.

Efavirenz becomes anionic at a pH range beyond its dual pKa values of 10.20 and 12.52, which is mainly responsible for the steep decline in

Table 6
Calculated interaction and binding energies of ARVDs onto various forms of graphene sheets.

Adduct	ΔE_{int}	ΔE_{bind}	Inter-molecular delocalized electrons		
	(kJ/mol)	*(kJ/mol)*	*Total*	*Dispersion*	*H-bonds*
NVP					
GW···NVP—H	–117.15	–104.27	0.94	0.94	0.00
GW···NVP$^-$	–99.66	–93.01	0.91	0.91	0.00
GW–NVP *(covalent)*	–95.10	+113.97			
GW(OH)···NVP-H	–149.49	–127.40	1.17	1.01	0.17
GW(OH)···NVP$^-$	–149.41	–126.23			
GW(O)···NVP$^-$	–100.04	–95.81			
EFV					
GW···EFV-H_2	–117.53	–112.30	1.01	1.01	0.00
GW···EFV^{2-}	–105.48	–94.94	0.97	0.97	0.00
GW(OH)···EFV-H_2	–145.39	–139.03			
GW(O)···EFV-H_2	–134.27	–125.69			
GW(O)···EFV^{2-}	–95.23	–89.87	1.19	1.14	0.05

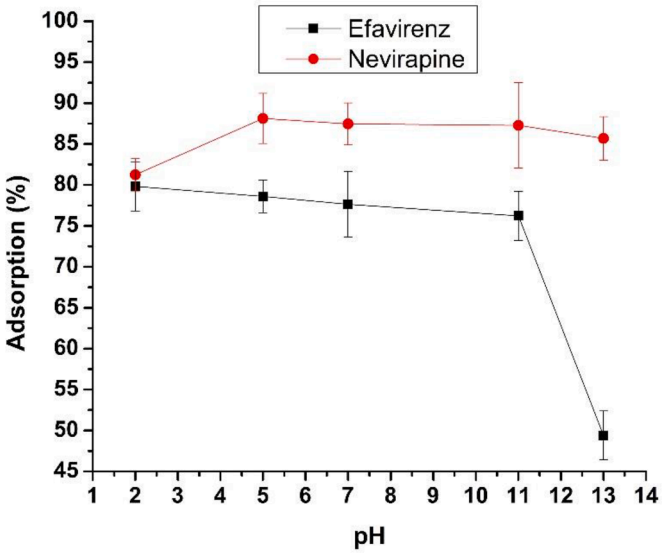

Fig. 6. Effect of pH on efavirenz and nevirapine adsorption onto graphene wool (Experimental conditions: Co = 5 mg/L; dosage = 10 mg per 10 mL solution, mixing rate = 200 rpm, $T = 25 \pm 1$ °C, contact time: 24 h). Error bars show ± relative standard deviation.

Table 5
Thermodynamic parameters for adsorption of efavirenz and nevirapine onto graphene wool (GW).

Temperature (K)	Efavirenz				Nevirapine			
	ln *b*	ΔG° (kJ/mol)	ΔH° (kJ/mol)	ΔS° (kJ/mol.K)	ln *b*	ΔG° (kJ/mol)	ΔH° (kJ/mol)	ΔS° (kJ/mol.K)
298	6.45	−15.98			10.36	−25.67		
308	11.52	−29.50	208.80	0.76	10.34	−26.48	−1.97	0.08
318	11.65	−30.80			10.31	−27.26		

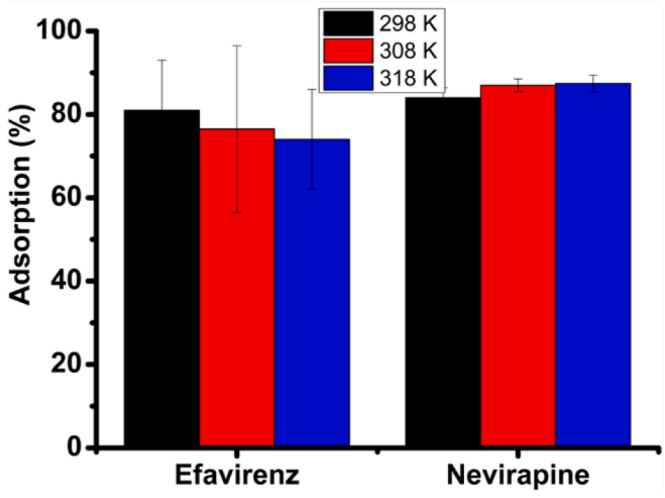

Fig. 7. Effect of temperature on adsorption performance of GW. Error bars show ±standard deviation $n = 5$. (Experimental conditions: $C_o = 1 - 20$ mg/L; dosage = 10 mg per 5 mL, mixing rate = 200 rpm, $T = 25 - 45$ °C).

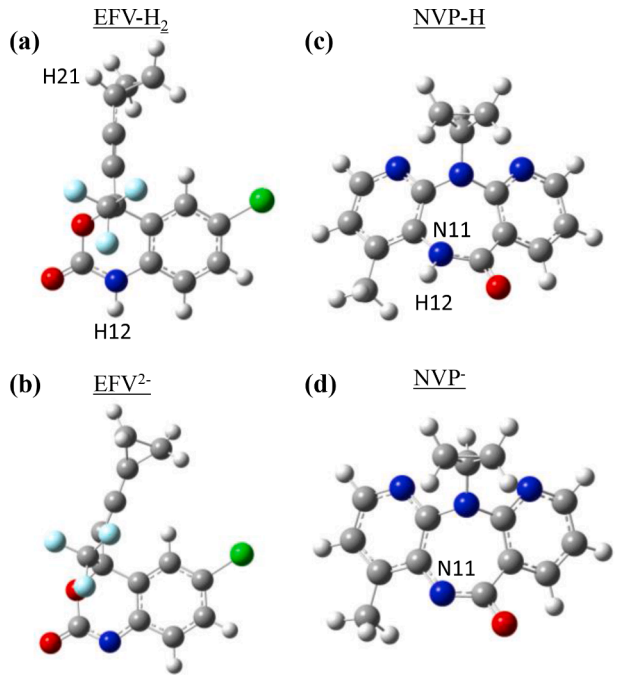

Fig. 8. DFT lowest-energy structures of protonated and deprotonated forms of efavirenz [EFV, (a) and (b)] and nevirapine [NVP, (c) and (d)]. Selected atoms and deprotonation sites are shown.

% adsorption in the basic medium. This is a result of electrostatic repulsion between the anionic EFV and deprotonated GW (negatively charged sorbent). The pKa of NVP is 2.8 and it is mainly anionic at pHs above its pKa value. This explains the slight increase in adsorption at acidic pH above its pKa (optimum at pH 5) because GW is protonated (positively charged) in an acidic medium, thus resulting in an attraction. A slight decline in adsorption at basic pH is due to weak electrostatic repulsion between the anionic NVP and negatively charged sorbent in the basic medium. The weak impact of electrostatic attraction and repulsion on NVP adsorption suggests that its adsorption onto GW is controlled by other mechanism(s) (Fig. 4) and electrostatic/van der Waal's attraction is complementary. A similar trend was reported for the adsorption of PCPPs such as carbamazepine, diclofenac, and clofibric acid by graphene oxide (GO) and chitosan [54, 55]

3.6. Adsorption thermodynamics and effect of temperature

Temperature plays a significant role in many physicochemical and biological processes. Adsorption thermodynamic parameters such as a change in enthalpy (ΔH), change in entropy (Δ*S*) and Gibbs free energy variation (ΔG), were derived from Van't Hoff equation eq. (14) and (15). The adsorption equilibrium constant (*b*) was deduced from the isotherm data using Eq. (11), at varying temperatures and used for the Van't Hoff plot (Fig. 7**b**) [50, 57]:

$$\ln b = \frac{\Delta S^{\circ}}{R} - \frac{\Delta H^{\circ}}{RT} \tag{14}$$

$$\Delta G^{\circ} = -RTln\ \ b \tag{15}$$

where ΔG is the change in the Gibbs free energy (kJ/mol); ΔH is the change in enthalpy (kJ/mol), and ΔS is the change in entropy (J/mol.K), R = gas constant (8.314 J/mol K), T = thermodynamic temperature (K). The value of b is derived from the Langmuir adsorption constant (K_L) by multiplying its value (in L/mg) by 1000 to convert the units to L/g, and then multiplied by the molar mass of the antiretroviral drug as stated in **Table 1**.

EFV adsorption is an endothermic process (ΔH) while NVP is exothermic (-ΔH) (**Table 5**). The negative ΔG and positive ΔS for GW-NVP and GW-EFV interactions confirm a spontaneous adsorption process, with an increase in spontaneity as temperature increases from 25 to 45 °C [21, 50]. The EFV adsorption diminished from 81% at room temperature to 74% at 45 °C, which could be attributed to a higher degree of disorderliness/randomness as temperature increased (Fig. 7). While NVP adsorption slightly improved from 84% at ambient temperature to 87% at 45 °C, which could be due to relatively lower net displacement in the sorbent-solution interphase (considering entropy values) [57]. The values of the adsorption equilibrium constant (ln *b*) and ΔG reveal that the impact of increasing temperature is more significant in GW-EFV interactions.

3.7. Computational studies of GW-EFV and GW-NVP interactions

Computational modelling using Density Functional Theory (DFT) was performed to assist with the interpretation of experimental results, as well as to further explore the interactions between EFV, NVP, and graphene wool. Optimized structures of protonated and deprotonated forms of EFV (EFV–H_2 and EFV^{2-}, respectively) and NVP (NVP–H and NVP^{-}, respectively) are shown in Fig. 8. The sequence of (de)protonation for each structure was established through the selection of the lowest energy tautomers of all possible ionized states; interestingly, the acidic proton associated with pKa = 10.20 in EFV was found to be –C≡≡C–C**H**$(CH_2)_2$ – H21 in Fig. 8**(a).**

Since the synthesized graphene wool contains C—O functional groups (XPS spectrum, Fig. 1**(b))**, graphene wool was modelled using three different structures: i) a single 5 × 5 graphene sheet, $C_{75}H_{17}$, labelled as GW, ii) a graphene sheet functionalized with a single O atom, labelled as GW(O) and iii) a graphene sheet functionalized with a single OH group, labelled as GW(OH). Constructing adducts of the absorbates and the three different forms of GW allow for a careful investigation of the effects of dispersion, electrostatics, covalent and non-covalent interactions. In particular, the *binding energy*,

$$\Delta E_{\text{bind}} = E(\text{adduct}) - E(\text{adsorbent}) - E(\text{adsorbate}) \tag{16}$$

calculates the adsorption energy relative to the lowest-energy, undeformed graphene sheet and adsorbates. In contrast, the *interaction energy*,

$$\Delta E_{\text{int}} = E(\text{adduct}) - E^{*}(\text{adsorbent}) - E^{*}(\text{adsorbate}) \tag{17}$$

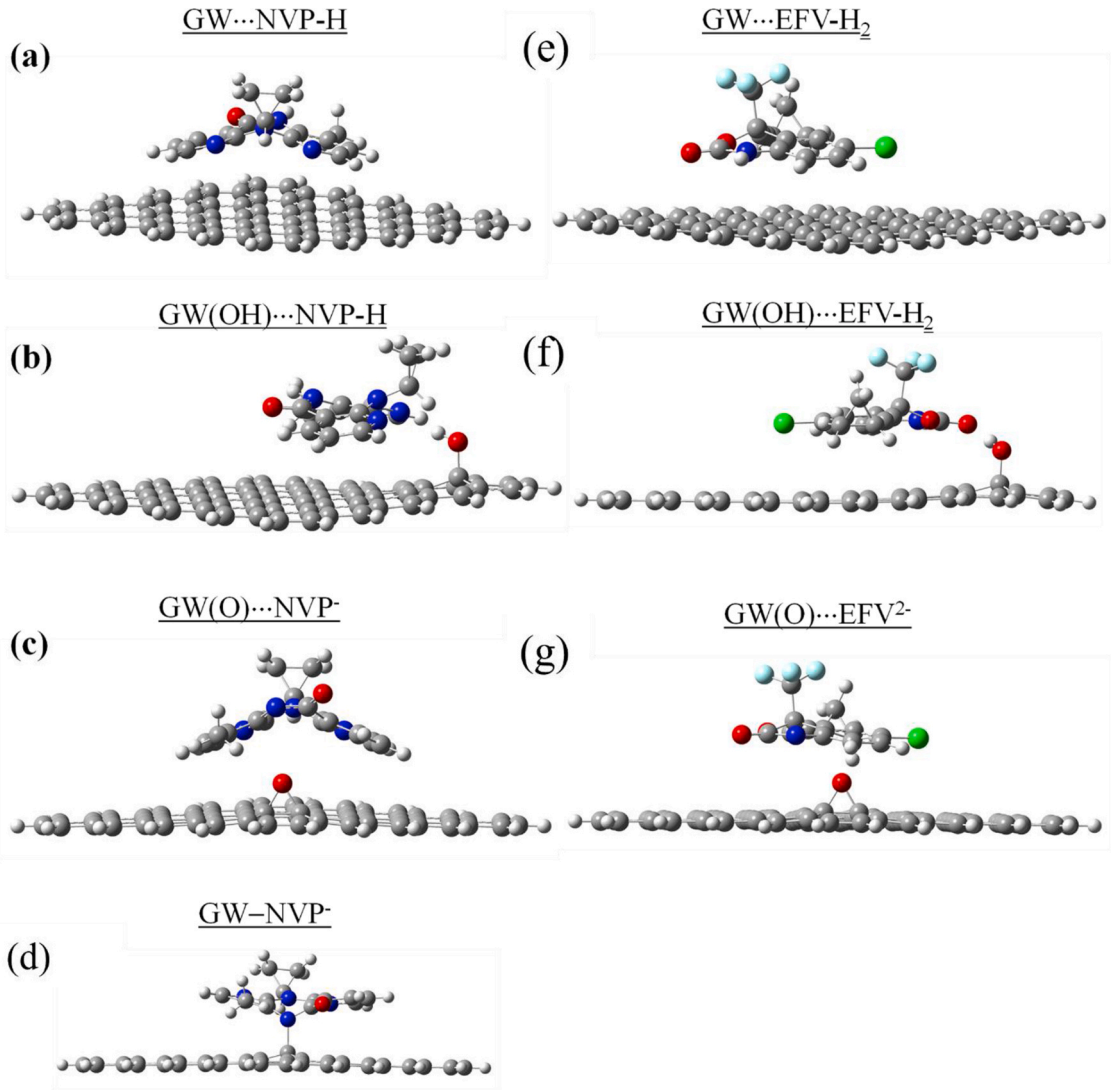

Fig. 9. DFT lowest-energy adducts between reduced graphene oxide (GW, graphene sheet), protonated and deprotonated graphene oxide (GW(OH), GW(O)) as adsorbents and various (de)protonated forms of EFV and NVP.

calculates the adsorption energy relative to the pre-organized, deformed molecules, where E°(adsorbent) and E°(adsorbate) are single-point structures in the geometry of the adsorbed adduct. The difference between ΔE_{bind} and ΔE_{int} is therefore the energy required to pre-organize the geometries of both adsorbent and adsorbate from their equilibrium structures to the conformations found in the adsorbed adduct, $\Delta E_{bind} = \Delta E_{int} + \Delta E_{org}(\text{adsorbent}) + \Delta E_{org}(\text{adsorbate})$.

The interactions between the ARVDs and the fully reduced GW are shown in Table 6. Interestingly, the neutral forms of NVP and EFV interact with a graphene sheet (Fig. 9) in a very comparable fashion (ΔE_{int}= –117.15 and –117.53 kJ/mol, respectively) given the parameters of the model: no functional groups present on a monolayer graphene sheet and lack of any cooperative effects. In these conditions, similar interaction energy indicates that the degree of dispersion and electrostatic interaction between GW and adsorbate is very similar for both NVP and EFV. However, NVP needs to deform more than EFV in order to adsorb to the GW surface, resulting in a slightly stronger overall binding energy for the adsorption of EFV (ΔE_{bind}= –104.27 and –112.30 kJ/mol for NVP and EFV, respectively). When both NVP and EFV are deprotonated, binding and interaction energies become less negative and indicate weaker adsorption. For instance, ΔE_{int} = –99.66 kJ/mol in the GW···NVP^{-} adduct, +17.49 kJ/mol higher than its neutral NVP-H counterpart. This observation therefore fully supports the reported experimental results, suggesting that negative charges on the deprotonated ARVDs leads to larger electrostatic repulsion with the generally electronegative graphene sheet.

It is plausible from the EFV···GW and NVP···GW interaction energies that these ARVDs adsorb to graphene primarily through dispersive interactions. The total number of electrons shared between each ARVD and the graphene sheet was modelled using FALDI and is tabulated in Table 6. NVP-H shares a surprisingly large total of 0.94 e^{-} (almost a full electron) with GW. However, no single diatomic contact makes a significant contribution – of a total of 3128 inter-molecular diatomic contacts in the GW···NVP-H adduct, the largest diatomic contribution is a fractional 0.023 e^{-} (3% of the total number of electrons shared), arising from a C···C contact (visualized in Fig. 10). Rather, the remarkable ability of graphene to delocalize electrons results in a strong dispersive interaction resulting from many, cumulative weak diatomic interactions. EFV-H_2 shares slightly more electrons with GW(O) (1.01 e^{-}) than NVP-H, indicating an even stronger dispersive interaction. On the other hand, the deprotonated forms of both ARVDs share slightly fewer electrons than their protonated counterparts. For instance, EFV^{2-} shares slightly fewer electrons (0.97 e^{-}) with the monolayer graphene sheet than EFV-H_2.

Low and high pH conditions can be simulated by considering the

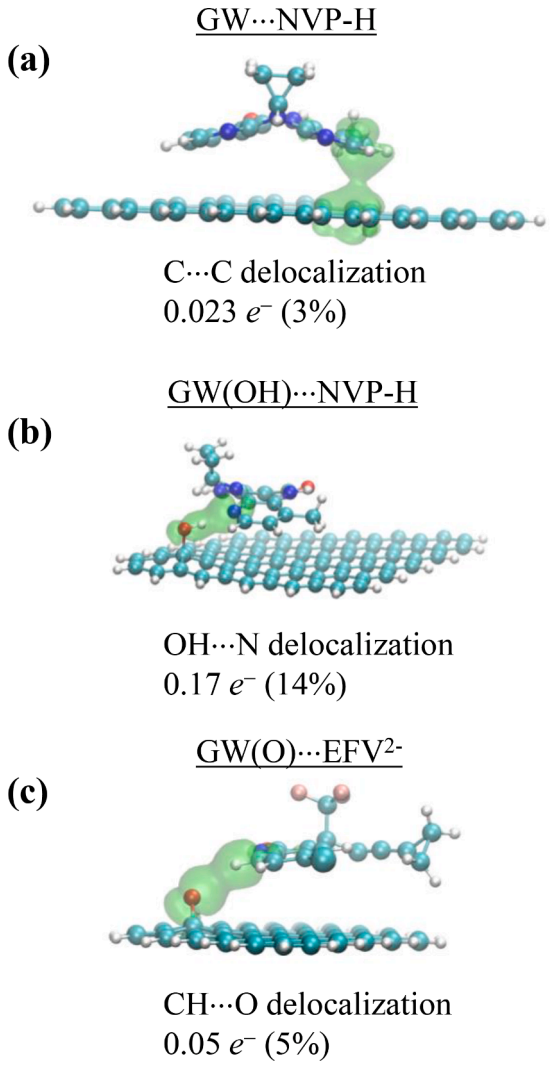

Fig. 10. DFT lowest-energy adducts between reduced graphene oxide (GW, graphene sheet), protonated and deprotonated graphene oxide [GW(OH), GW (O)] as absorbates and various (de)protonated forms of EFV and NVP.

functionalized GW model, either as GW(OH) or GW(O), respectively. When the graphene sheet is functionalized in this manner, results in Table 6 display a slightly different picture. The interaction and binding energies of NVP-H are stabilized when adsorbing to a GW(OH), ΔE_{bind}= –127.40 kJ/mol for GO(OH)···NVP-H, –23.14 kJ/mol lower than for rGO···NVP-H. Very similar values are observed for the deprotonated GW (OH)···NVP$^-$ adduct. The origin of this stabilization in functionalized graphene relative to a reduced GW is clearly an OH···N hydrogen-bond (Fig. 9(b)), which is confirmed with FALDI – an additional 0.17 e^- are shared amongst the relevant O, H, and N atoms (visualized in **Fig. 10 (b)**). At high pH conditions, the GW(OH) sheet is expected to be deprotonated to GW(O). As a result, the GW(O)···NVP$^-$ interaction is destabilized (ΔE_{bind}= −95.81 kJ/mol) relative to GW(OH)···NVP-H and is very similar to the GW···NVP$^-$ adduct, due to a lack of any significant H-bonding. Of particular note, however, is the interaction of EFV with GW(OH) and GW(O). When both absorbent and absorbate are protonated (as expected for low pH conditions), the GW(OH)···EFV-H_2 interaction is the strongest out of all adducts investigated (ΔE_{bind}= –33.23 kJ/mol). However, as the graphene sheet and EFV molecule are deprotonated, the adduct is destabilized: ΔE_{bind}= +13.39 kJ/mol higher in GW(O)···EFV-H_2 and +49.20 kJ/mol higher in the fully protonated GW(O)···EFV^{2-}. This result fully supports the presented experimental findings that the degree of adsorption of EFV decreases at high pH, Fig. 6. It also lends credence that EFV is predominantly adsorbed through dispersion interactions with graphene at neutral and basic pH conditions. A weak CH···O interaction is detected in the GW(O)···EFV^{2-} adduct, but it only contributes 0.05 e^- to the total number of delocalized electrons (**Fig. 10(c)**). Interestingly, the total number of delocalized electrons due to dispersion is the highest in GW(O)···EFV^{2-} of all adducts investigated (1.14 e^-) which, in conjunction with the relatively destabilized binding energy, indicates a significant degree of electrostatic repulsion is present.

Finally, we have only been able to find a single adduct with a *covalent* bond between adsorbate and graphene. Specifically, NVP$^-$ can bind through the deprotonated nitrogen atom (N11, **Fig. 8(c)**) to form the GW–NVP$^-$ covalently bonded complex, **Fig. 9(d)**. The structure is metastable, however, in a very shallow potential energy well. All other candidate covalent adducts, including all forms of EFV and other conformations of NVP with graphene, were disregarded as unlikely due to extremely large binding energies at average covalent bond distances. The GW–NVP$^-$ complex is characterized by moderately negative interaction energy (ΔE_{int}= –95.10 kJ/mol) but positive binding energy (ΔE_{bind} = +113.97 kJ/mol), Table 6. Our modelling therefore suggests that the graphene–NVP$^-$ covalent bond is attractive but requires large deformations in both adsorbate and absorbent in order to form. In addition, as we did not find any other structures which seems to support covalent bonding with graphene, it is highly probable that the observed covalent bond is a feature exclusive to the deprotonated form of NVP$^-$. It is very likely that a more complex model including e.g., multiple graphene layers, the inclusion of defects or increased graphene functionalization will further stabilize this covalent complex, but such modelling lies outside of the scope of this work.

Conclusion

A comprehensive risk-based assessment of graphene is currently unavailable; however, many researchers believe that the material does not pose a high health risk based on its composition, but it may pose a potential risk as a result of its thin and lightweight nature. Particularly, graphene in the particulate form could prove worrisome regarding inhalation risks. The physical structure of the graphene-based material and the fabrication method is therefore critical. With respect to graphene wool, the quartz wool substrate acts as solid support, assisting with immobilization of the graphene. This study revealed that graphene wool can be used as an effective adsorbent for the removal of antiretroviral drug contaminants, specifically efavirenz and nevirapine from aqueous solution. The Sips, Freundlich, pseudo-second-order, and intraparticle diffusion adsorption models best describe the sorption processes, and experimental variables such as pH and temperature only slightly influence nevirapine adsorption. This suggests that its interaction is majorly controlled by strong electronic interaction between moieties containing lone pairs leading to hydrogen bonding, and π-π stacking between GW and NVP. It could be concluded that GW-EFV interaction is comparably weaker, with less hysteresis and higher desorption potential, and is controlled by hydrophobic and electrostatic interactions. Computational studies suggest that both GW···EFV and GW···NVP interactions are predominantly controlled by dispersive interactions, although specific (de)protonation of functional groups on the graphene layer can lead to significant additional stabilization through hydrogen bonds. This study presents the first experimental and computational investigation of the potential application of a graphene-based material (graphene wool) as an efficient next-generation sorbent for the removal of antiretroviral drug contamination in water. Furthermore, unlike most graphene generated in the form of flakes or powder, graphene wool provides a wool-like form that may be more suitable as a packing material for filters and other water polishing tools. The synthesis of graphene wool is facile and eco-friendly without extensive use of chemicals. Therefore, under appropriate operating conditions, the graphene wool adsorbent can potentially be utilized as a water polishing

tool for the removal of antiretroviral drug contaminants and other organic chemical pollutants.

Conflict of interest

The authors declare that there is no conflict of interest regarding the publication of this article.

Declaration of Competing Interests

The authors declare that they have no known competing financial interests or personal relationships that could have appeared to influence the work reported in this paper.

Acknowledgements

Authors acknowledge the University of Pretoria Commonwealth Doctoral Scholarship (AA) and the Rand Water Professorial Chair program (PF) for providing funding for this research.

References

[1] M. Parolini, A. Pedriali, A. Binelli, Application of a biomarker response index for ranking the toxicity of five pharmaceutical and personal care products (PPCPs) to the bivalve dreissena polymorpha, Arch. Environ. Contam. Toxicol. 64 (2013) 439–447, https://doi.org/10.1007/s00244-012-9847-3.

[2] A.J. Ebele, M. Abou-Elwafa Abdallah, S. Harrad, Pharmaceuticals and personal care products (PPCPs) in the freshwater aquatic environment, Emerg. Contam. 3 (2017) 1–16, https://doi.org/10.1016/j.emcon.2016.12.004.

[3] B. Petrie, R. Barden, B. Kasprzyk-Hordern, A review on emerging contaminants in wastewaters and the environment: current knowledge, understudied areas and recommendations for future monitoring, Water Res 72 (2015) 3–27, https://doi.org/10.1016/j.watres.2014.08.053.

[4] A.O. Adeola, P.B. Forbes, Antiretroviral drugs in african surface waters: prevalence, analysis, and potential remediation, Environ Toxicol Chem (2021), https://doi.org/10.1002/etc.5127.

[5] J. Funke, C. Prasse, T.A. Ternes, Identification of transformation products of antiviral drugs formed during biological wastewater treatment and their occurrence in the urban water cycle, Water Res 98 (2016) 75–83, https://doi.org/10.1016/j.watres.2016.03.045.

[6] C. Prasse, M.P. Schlüsener, R. Schulz, T.A. Ternes, Antiviral drugs in wastewater and surface waters: a new pharmaceutical class of environmental relevance? Environ. Sci. Technol. 44 (2010) 1728–1735, https://doi.org/10.1021/es903216p.

[7] A.J. Al-Rajab, L. Sabourin, R. Chapman, D.R. Lapen, E. Topp, Fate of the antiretroviral drug tenofovir in agricultural soil, Sci. Total Environ. 408 (2010) 5559–5564, https://doi.org/10.1016/j.scitotenv.2010.07.074.

[8] M. Wooding, E.R. Rohwer, Y. Naudé, Determination of endocrine disrupting chemicals and antiretroviral compounds in surface water: a disposable sorptive sampler with comprehensive gas chromatography – time-of-flight mass spectrometry and large volume injection with ultra-high performance liquid chromatography–tandem mass spectrometry, J. Chromatogr. A. 1496 (2017) 122–132, https://doi.org/10.1016/j.chroma.2017.03.057.

[9] C. Schoeman, M.Mashiane C, M. Dlamini, O.J. Okonkwo, Quantification of selected antiretroviral drugs in a wastewater treatment works in South Africa using GC-TOFMS, J. Chromatogr. Sep. Tech. 6 (2015) 272, https://doi.org/10.4172/2157-7064.1000272.

[10] G. Mascolo, L. Balest, D. Cassano, G. Laera, A. Lopez, A. Pollice, C. Salerno, Biodegradability of pharmaceutical industrial wastewater and formation of recalcitrant organic compounds during aerobic biological treatment, Bioresour. Technol. 101 (2010) 2585–2591, https://doi.org/10.1016/j.biortech.2009.10.057.

[11] E. Ngumba, A. Gachanja, T. Tuhkanen, Occurrence of selected antibiotics and antiretroviral drugs in Nairobi River Basin, Kenya, Sci. Total Environ. 539 (2016) 206–213, https://doi.org/10.1016/j.scitotenv.2015.08.139.

[12] D. Gökengin, F. Doroudi, J. Tohme, B. Collins, N. Madani, HIV/AIDS: trends in the Middle East and North Africa region, Int. J. Infect. Dis. 44 (2016) 66–73, https://doi.org/10.1016/j.ijid.2015.11.008.

[13] S. Ncube, L.M. Madikizela, L. Chimuka, M.M. Nindi, Environmental fate and ecotoxicological effects of antiretrovirals: a current global status and future perspectives, Water Res 145 (2018) 231–247, https://doi.org/10.1016/j.watres.2018.08.017.

[14] J.L. Tambosi, L.Y. Yamanaka, H.J. José, R.d.F.P.M. Moreira, H.F. Schröder, Recent research data on the removal of pharmaceuticals from sewage treatment plants (STP), Quím. Nova 33 (2010) 411–420, https://doi.org/10.1590/S0100-40422010000200032.

[15] B. Halling-Sørensen, S. Nors Nielsen, P.F. Lanzky, F. Ingerslev, H.C. Holten Lützhøft, S.E. Jørgensen, Occurrence, fate and effects of pharmaceutical substances in the environment- a review, Chemosphere 36 (1998) 357–393, https://doi.org/10.1016/S0045-6535(97)00354-8.

[16] G. Kumari, R.K. Singh, Highly active antiretroviral therapy for treatment of HIV/AIDS patients: current status and future prospects and the Indian scenario, HIV & AIDS Rev. 11 (2012) 5–14, https://doi.org/10.1016/j.hivar.2012.02.003.

[17] C. Schoeman, M. Dlamini, O.J. Okonkwo, The impact of a wastewater treatment works in southern Gauteng, South Africa on efavirenz and nevirapine discharges into the aquatic environment, Emerg. Contam. 3 (2017) 95–106, https://doi.org/10.1016/j.emcon.2017.09.001.

[18] K.O. K'Oreje, L. Vergeynst, D. Ombaka, P. De Wispelaere, M. Okoth, H. Van Langenhove, K. Demeestere, Occurrence patterns of pharmaceutical residues in wastewater, surface water and groundwater of Nairobi and Kisumu city, Kenya, Chemosphere 149 (2016) 238–244, https://doi.org/10.1016/j.chemosphere.2016.01.095.

[19] S.-J. Zou, Y.-F. Chen, Y. Zhang, X.-F. Wang, N. You, H.-T. Fan, A hybrid sorbent of α-iron oxide/reduced graphene oxide: studies for adsorptive removal of tetracycline antibiotics, J. Alloys Compd. 863 (2021), 158475.

[20] Y.-X. Song, S. Chen, N. You, H.-T. Fan, L.-N. Sun, Nanocomposites of zero-valent iron@activated carbon derived from corn stalk for adsorptive removal of tetracycline antibiotics, Chemosphere 255 (2020), 126917.

[21] S.-J. Zou, B.-H. Ding, Y.-F. Chen, H.-T. Fan, Nanocomposites of graphene and zirconia for adsorption of organic-arsenic drugs: performances comparison and analysis of adsorption behavior, Environ. Res. 195 (2021), 110752.

[22] A.O. Adeola, P.B.C. Forbes, Advances in water treatment technologies for removal of polycyclic aromatic hydrocarbons: existing concepts, emerging trends, and future prospects, Water Environ. Res. 93 (3) (2021) 343–359, https://doi.org/10.1002/wer.1420.

[23] N. You, X.-F. Wang, J.-Y. Li, H.-T. Fan, H. Shen, Q. Zhang, Synergistic removal of arsanilic acid using adsorption and magnetic separation technique based on Fe_3O_4@graphene nanocomposite, J. Indust. Eng. Chem. 70 (2019) 346–354.

[24] D. Balarak, G. McKay, Utilization of MWCNTs/Al2O3 as adsorbent for ciprofloxacin removal: equilibrium, kinetics and thermodynamic studies, J. Environ. Sci. Health A. 56 (3) (2021) 324–333, https://doi.org/10.1080/10934529.2021.1873674.

[25] PubChem, Bethesda (MD): National Library of Medicine (US), National Center For Biotechnology Information, PubChem Compound Summary for CID, 2004, p. 4463. Nevirapine; [cited 2020 Aug. 10]. Available from: https://pubchem.ncbi.nlm.nih.gov/compound/Nevirapine.

[26] PubChem, Bethesda (MD): National Library of Medicine (US), National Center For Biotechnology Information, PubChem Compound Summary for CID, 2004, p. 64139. Efavirenz; [cited 2020 Aug. 10]. Available from: https://pubchem.ncbi.nlm.nih.gov/compound/Efavirenz.

[27] G.-L. Schoonraad, M.J. Madito, N. Manyala, P. Forbes, Synthesis and optimisation of a novel graphene wool material by atmospheric pressure chemical vapour deposition, J. Mater. Sci. 55 (2020) 545–564, https://doi.org/10.1007/s10853-019-03948-0.

[28] Gaussian 16, Revision C.01, M. J. Frisch, G. W. Trucks, H. B. Schlegel, G. E. Scuseria, M. A. Robb, J. R. Cheeseman, G. Scalmani, V. Barone, G. A. Petersson, H. Nakatsuji, X. Li, M. Caricato, A. V. Marenich, J. Bloino, B. G. Janesko, R. Gomperts, B. Mennucci, H. P. Hratchian, J. V. Ortiz, A. F. Izmaylov, J. L. Sonnenberg, D. Williams-Young, F. Ding, F. Lipparini, F. Egidi, J. Goings, B. Peng, A. Petrone, T. Henderson, D. Ranasinghe, V. G. Zakrzewski, J. Gao, N. Rega, G. Zheng, W. Liang, M. Hada, M. Ehara, K. Toyota, R. Fukuda, J. Hasegawa, M. Ishida, T. Nakajima, Y. Honda, O. Kitao, H. Nakai, T. Vreven, K. Throssell, J. A. Montgomery, Jr., J. E. Peralta, F. Ogliaro, M. J. Bearpark, J. J. Heyd, E. N. Brothers, K. N. Kudin, V. N. Staroverov, T. A. Keith, R. Kobayashi, J. Normand, K. Raghavachari, A. P. Rendell, J. C. Burant, S. S. Iyengar, J. Tomasi, M. Cossi, J. M. Millam, M. Klene, C. Adamo, R. Cammi, J. W. Ochterski, R. L. Martin, K. Morokuma, O. Farkas, J. B. Foresman, and D. J. Fox, Gaussian, Inc., Wallingford CT, 2016.

[29] J.H. de Lange, I. Cukrowski, Toward deformation densities for intramolecular interactions without radical reference states using the fragment, atom, localized, delocalized and interatomic (FALDI) charge density decomposition scheme, J. Comput. Chem. 38 (2017) 981–997, https://doi.org/10.1002/jcc.24772.

[30] J.H. de Lange, I. Cukrowski, Exact and exclusive electron localization indices within QTAIM atomic basins, J. Comput. Chem. 39 (2018) 1517–1530, https://doi.org/10.1002/jcc.25223.

[31] R.F. Bader, Atoms in Molecules, Wiley Online Library, 2020.

[32] AIMAll (Version 19.10.12), Todd A. Keith, TK Gristmill software, Overland Park KS, USA, 2019 (aim.tkgristmill.com).

[33] W. Humphrey, A. Dalke, K. Schulten, VMD: visual molecular dynamics, J. Mol. Graph. 14 (1996) 33–38, https://doi.org/10.1016/0263-7855(96)00018-5.

[34] G.A. Haghighat, M.H. Saghi, I. Anastopoulos, A. Javid, A. Roudbari, S.S. Talebi, S. K. Ghadiri, D.A. Giannakoudakis, M. Shams, Aminated graphitic carbon derived from corn stover biomass as adsorbent against antibiotic tetracycline: optimizing the physicochemical parameters, J. Mol. Liq. 313 (2020), 113523, https://doi.org/10.1016/j.molliq.2020.113523.

[35] F.T. Johra, J.-W. Lee, W.-G. Jung, Facile and safe graphene preparation on solution based platform, J. Ind. Eng. Chem. 20 (2014) 2883–2887, https://doi.org/10.1016/j.jiec.2013.11.022.

[36] M.V. Khedkar, S.B. Somvanshi, A.V. Humbe, K.M. Jadhav, Surface modified sodium silicate based superhydrophobic silica aerogels prepared via ambient pressure drying process, J. Non-Cryst. Solids 511 (2019) 140–146, https://doi.org/10.1016/j.jnoncrysol.2019.02.004.

[37] J. Chen, W. Chen, D. Zhu, Adsorption of nonionic aromatic compounds to single-walled carbon nanotubes: effects of aqueous solution chemistry, Environ. Sci. Technol. 42 (2008) 7225–7230, https://doi.org/10.1021/es801412j.

[38] Y. Huang, J. Tang, L. Gai, Y. Gong, H. Guan, R. He, H. Lyu, Different approaches for preparing a novel thiol-functionalized graphene oxide/Fe-Mn and its application

for aqueous methylmercury removal, Chem. Eng. J. 319 (2017) 229–239, https://doi.org/10.1016/j.cej.2017.03.015.
[39] A.A. Mirghni, K.O. Oyedotun, B.A. Mahmoud, A. Bello, S.C. Ray, N. Manyala, Nickel-cobalt phosphate/graphene foam as enhanced electrode for hybrid supercapacitor, Compos. B. Eng. 174 (2019), 106953, https://doi.org/10.1016/j.compositesb.2019.106953.
[40] E.T. Anthony, M.O. Ojemaye, A.I. Okoh, O.O. Okoh, Synthesis of CeO2 as promising adsorbent for the management of free-DNA harboring antibiotic resistance genes from tap-water, Chem. Eng. J. 401 (2020), 125562, https://doi.org/10.1016/j.cej.2020.125562.
[41] A.O. Adeola, P.B.C. Forbes, Optimization of the sorption of selected polycyclic aromatic hydrocarbons by regenerable graphene wool, Water Sci. Technol. 80 (2019) 1931–1943, https://doi.org/10.2166/wst.2020.011.
[42] W.J. Weber, E.H. Smith, Simulation and design models for adsorption processes, Environ. Sci. Technol. 21 (1987) 1040–1050, https://doi.org/10.1021/es00164a002.
[43] F. Yu, J. Ma, D. Bi, Enhanced adsorptive removal of selected pharmaceutical antibiotics from aqueous solution by activated graphene, Environ. Sci. Pollut. Res. 22 (2015) 4715–4724, https://doi.org/10.1007/s11356-014-3723-9.
[44] E.E. Jasper, V.O. Ajibola, J.C. Onwuka, Nonlinear regression analysis of the sorption of crystal violet and methylene blue from aqueous solutions onto an agro-waste derived activated carbon, Appl. Water Sci. 10 (2020) 132, https://doi.org/10.1007/s13201-020-01218-y.
[45] K.Y. Foo, B.H. Hameed, Insights into the modeling of adsorption isotherm systems, Chem. Eng. J. 156 (2010) 2–10, https://doi.org/10.1016/j.cej.2009.09.013.
[46] B. Nagy, C. Mânzatu, A. Măicăneanu, C. Indolean, L. Barbu-Tudoran, C. Majdik, Linear and nonlinear regression analysis for heavy metals removal using Agaricus bisporus macrofungus, Arab. J. Chem. 10 (2017) S3569–S3579, https://doi.org/10.1016/j.arabjc.2014.03.004.
[47] X.-J. Zhao, H. Hou, X.-T. Fan, Y. Wang, Y.-M. Liu, C. Tang, S.-H. Liu, P.-P. Ding, J. Cheng, D.-H. Lin, C. Wang, Y. Yang, Y.-Z. Tan, Molecular bilayer graphene, Nat. Commun. 10 (2019) 3057, https://doi.org/10.1038/s41467-019-11098-9.
[48] V. Georgakilas, J.N. Tiwari, K.C. Kemp, J.A. Perman, A.B. Bourlinos, K.S. Kim, R. Zboril, Noncovalent functionalization of graphene and graphene oxide for energy materials, biosensing, catalytic, and biomedical Applications, Chem. Rev. 116 (2016) 5464–5519, https://doi.org/10.1021/acs.chemrev.5b00620.
[49] D. Hao, Y.-X. Song, Y. Zhang, H.-T. Fan, Nanocomposites of reduced graphene oxide with pure monoclinic-ZrO_2 and pure tetragonal-ZrO_2 for selective adsorptive removal of oxytetracycline, Appl. Surf. Sci. 543 (2021), 148810.
[50] A.R.D. Verliefde, E.R. Cornelissen, S.G.J. Heijman, J.Q.J.C. Verberk, G.L. Amy, B. Van der Bruggen, J.C. van Dijk, The role of electrostatic interactions on the rejection of organic solutes in aqueous solutions with nanofiltration, J. Membr. Sci. 322 (2008) 52–66, https://doi.org/10.1016/j.memsci.2008.05.022.
[51] A.O. Adeola, P.B.C. Forbes, Influence of natural organic matter fractions on PAH sorption by stream sediments and a synthetic graphene wool adsorbent, Environ. Technol. Innovat. 21 (2021), 101202, https://doi.org/10.1016/j.eti.2020.101202.
[52] J. Li, C. Chen, S. Zhang, X. Ren, X. Tan, X. Wang, Critical evaluation of adsorption–desorption hysteresis of heavy metal ions from carbon nanotubes: influence of wall number and surface functionalization, Chem. Asian J. 9 (2014) 1144–1151, https://doi.org/10.1002/asia.201301475.
[53] C. Tesseromatis, A. Alevizou, The role of the protein-binding on the mode of drug action as well the interactions with other drugs, Eur. J. Drug Metab. Ph. 33 (2008) 225–230, https://doi.org/10.1007/BF03190876.
[54] Y. Zhang, Z. Shen, C. Dai, X. Zhou, Removal of selected pharmaceuticals from aqueous solution using magnetic chitosan: sorption behavior and mechanism, Environ. Sci. Pollut. Res. 21 (2014) 12780–12789, https://doi.org/10.1007/s11356-014-3212-1.
[55] T.J. Al-Musawi, A.H. Mahvi, A.D. Khatibi, D. Balarak, Effective adsorption of ciprofloxacin antibiotic using powdered activated carbon magnetized by iron(III) oxide magnetic nanoparticles, J. Porous Mater. 28 (2021) 835–852, https://doi.org/10.1007/s10934-021-01039-7.
[56] Y. Liu, Is the free energy change of adsorption correctly calculated? J. Chem. Eng. Data 54 (2009) 1981–1985.
[57] L. Wang, C. Shi, L. Wang, L. Pan, X. Zhang, J.-J. Zou, Rational design, synthesis, adsorption principles and applications of metal oxide adsorbents: a review, Nanoscale 12 (2020) 4790–4815, https://doi.org/10.1039/C9NR09274A.